Dynamic erosion of plasma facing materials under ITER relevant thermal shock loads in the electron beam facility, JUDITH

T. Hirai, W. Kühnlein, J. Linke, G. Sergienko

Forschungszentrum Jülich GmbH, EURATOM Association, 52425 Jülich, Germany

e-mail contact of main author: t.hirai@fz-juelich.de

Abstract. ITER relevant thermal shock loads have been performed in the electron beam facility, JUDITH. Dynamic erosion processes of fine grain graphite, carbon fiber composite (CFC) and W-1%La$_2$O$_3$ were observed by optical diagnostics. Collective small particle release which may correspond to erosion of graphite binder phase was observed at 2 GW/m^2 in graphite, whereas, distinguished particle release was observed at the same power density in CFC. The distinguished particle release was concluded to be due to brittle destruction of overheated PAN fibers which has lower thermal conductivity in vertical direction. Most particles released from W-1%La$_2$O$_3$ were appeared to be droplets splashed from the molten surface. The contribution of brittle destruction in W-1%La$_2$O$_3$ was not clearly observed in this particular thermal shock loads. Release of tungsten atoms and WO molecules was not observed by emission spectrometer even at high power density, 1.1 GW/m^2 which caused melting of the surfaces, however, release of LaO molecules was detected even at lower power density, 0.6 GW/m^2 where and the surface did not show significant modification.

1. Introduction

Thermal shock loads in the order of several 10 MJ/m^2 with duration of a few ms (plasma disruptions) are predicted in ITER [1]. Carbon based materials (carbon fiber composite: CFC) had been selected as plasma facing armor materials in ITER divertor since it has a high thermal shock resistance and high thermal conductivity. However, recent studies show a strong erosion of carbon based materials due to macroscopic erosion caused by brittle destruction (BD) under plasma disruption condition [2-9]. Macroscopic erosion is associated with a substantial material loss because the released particles are not re-deposited on surfaces but create directly dusts. Moreover, brittle materials such as tungsten and the alloys that are the other ITER candidate materials in the divertor, are also concerned from a view point of material loss due to BD. Therefore, the detailed studies of material erosion under thermal shock loads are necessary. In the present paper, dynamic erosion processes of plasma facing materials under intense thermal loads were studied by newly developed optical diagnostics.

2. Experiments
2.1 Electron beam facility, JUDITH

Thermal shock experiments were carried out in the electron beam facility, JUDITH (JUelicher DIvertor Test facility in Hot cells) [10]. The picture and schematic view are depicted in figure 1. Advantages of high heat flux testing by electron beam are the flexible operation (pulse length: ~1 ms up to continuous work) and homogeneous heat loading on large areas. Thermal shock tests have been carried out in electron beam facilities, JUDITH [2-9], JEBIS [11] and OHBIS [12] by using capacitor modes, i.e. short pulse modes. The power density is limited by maximum beam currents, acceleration voltages and minimum diameters of the beam spot. A relatively high acceleration voltage is used in electron beam facilities in order to achieve the high power with a limited beam current. The disadvantages are relatively large penetration depth caused by the high acceleration voltage, high energy reflection and no possibility to apply magnetic fields around the targets. The large penetration depth causes volumetric heating rather than surface heating in the targets (120 keV electrons can penetrate 100 μm in carbon materials). Furthermore, a heat flux of energetic electrons will not be influenced by vapor clouds created in front of targets. The vapor clouds are considered to reduce significant heat influx due to the heat flux shielding effect [13]. Consequently, the thermal shock tests by energetic electron beam might overestimate the erosion rate compared with plasma disruption in tokamaks. Nevertheless, it is worth using electron beam facilities for systematic studies of material behavior under thermal shock loads.

The electron beam facility, JUDITH, is installed in hot cell laboratory, which enable to perform thermal shock tests on neutron-irradiated and toxic materials, like beryllium. It is a great advantage to investigate full variety of ITER candidate materials including neutron-irradiated samples. The target samples are loaded in a vacuum by an energetic electron beam (120 keV). The electron beam had a full width half maximum (FWHM) of about 1 mm at the target and the beam was scanned typically with 30-40 kHz on the surface to obtain homogeneous thermal loads. The incident power density achieves up to 15 GW/m^2 in this facility.
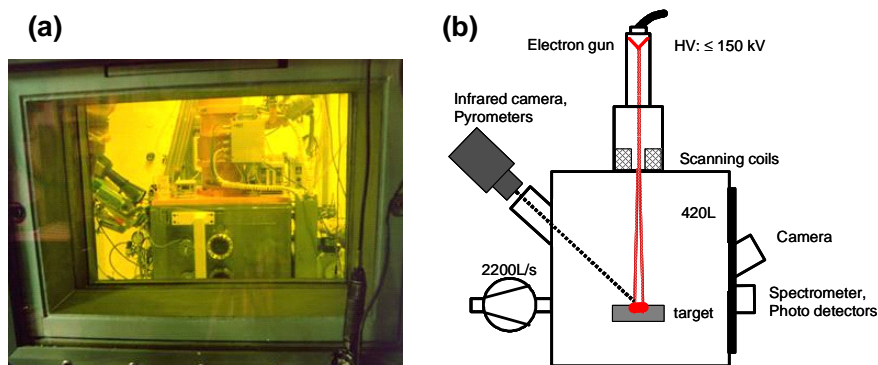

Fig. 1 Electron beam facility, JUDITH, (a) view from the outside the hot cell, (b) the schematic drawing.
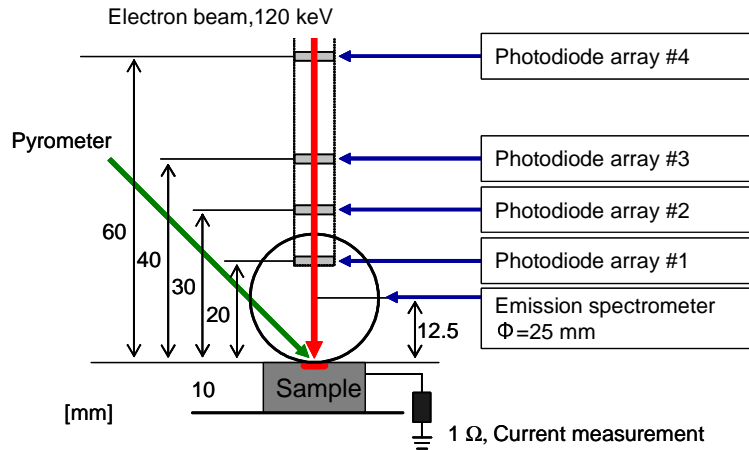
Fig. 2, Observing volumes of optical diagnostics in JUDITH.

2.2 Diagnostics

In order to observe the dynamic erosion processes, optical diagnostics have been developed. The erosion processes under thermal shock loads can be roughly classified into two processes: macroscopic and microscopic erosion. The macroscopic erosion corresponds to particle release due to brittle destruction and/or splashing of molten surface. It was observed by photodiode array (PDA) aligned above the target surface. Thermal radiation from hot particles was detected by the PDA with near-infrared cut-off filter (850 nm). The observing volume is 1.8 x 7.6 mm (shown in figure 2) at 4 different points along the electron beam axis. The microscopic erosion corresponds to releases of atomic and molecular components due to sublimation or evaporation at high temperatures. It was detected by emission spectrometer. Emission spectrometer could detect ultraviolet (200 nm) to infrared (1000 nm), however, the transmission of optics and optical fiber limited the observing wavelength in a visible range (380 nm - 800 nm). The observing volumes are shown in figure 2. A single color pyrometer was pointing at the loaded hot surface with an observing area of $\phi \sim 4$ mm. The pyrometer provided an average surface temperature in the observing area. Emissivity was fixed at values of 0.9 for carbon based materials and 0.3 for W-1%La$_2$O$_3$. Consequently, the measuring temperatures were 600 - 4000 ^{o}C in case of carbon based materials and above 700 ^{o}C in case of tungsten alloy. Current measurements were also performed to monitor "absorbed current" (electric current through the samples) by measuring the electric potential of a grounded resistor (1 Ω).

2.3 Samples and experimental conditions

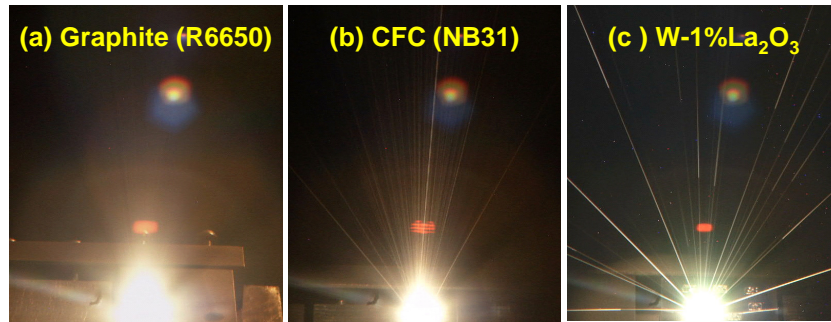Fine grain graphite (R6650, SGL-Carbon), CFC (NB31, SNECMA Motors) and W-1%La$_2$O$_3$

Fig.3, time integral image during thermal shock tests on (a) graphite, 2 GW/m^2, 4.6 ms, (b) CFC, 2 GW/m^2, 4.6ms, (c) W-1%La$_2$O$_3$, 1.1 GW/m^2, 4.6 ms.

(Plansee) with dimensions of 25 x 25 x 10 mm^3, were loaded by the electron beam at room temperature. The loading power density and the duration were 0.6 - 2 GW/m^2 and 4.6 ms, respectively. All high power density shots were applied on small areas (~16 mm^2), therefore, the increase of bulk temperature was negligible.

3. Results and discussion
3.1 Thermal shock tests on carbon based materials, graphite and CFC

In case of graphite, two components of particle release due to brittle destruction were considered: large particles and small particles which are corresponding to graphite grain clusters and binder phase, respectively [5,8,9]. At the present power density, faint traces were observed as shown in Fig. 3(a). This is the small particle release from graphite target. The surface temperature reached above 3000 ^{o}C in the thermal shock test (Fig. 4(a)). Absorbed current started to drop around 2000 ^{o}C and the current exceeded zero point to negative after the shot (Fig. 4(b)). It is caused by thermal electron emission from the hot surface. According to the surface temperature excursion, there was not significant disturbance from the thermally emitted electron since the experiments were performed with energetic electron beam (120keV). As can be expected by the collective release of small particles, continuum was observed in PDA signals (Fig. 4(c)). All signals started to appear around 3 ms when the surface temperature was high enough (>2500°C) and disappear immediately after the shot. These results indicate relatively fast speed of released particles [9].

CFC showed particle release due to brittle destruction at power density 2 GW/m^2 (see bright traces in Fig. 3(b)). The PDA signals showed rather distinguished particle release (Fig. 4(f)). The maximum surface temperature was around 2500 ^{o}C. This was lower than graphite. However, one should note that the temperature is averaged over the observing area. The particular CFC, NB31, has ex-pitch fibers with high thermal conductivity and PAN fibers with lower thermal conductivity in the vertical direction. The local overheating could apparently occur at PAN fibers. In fact, pitch fiber did not show remarkable modification,
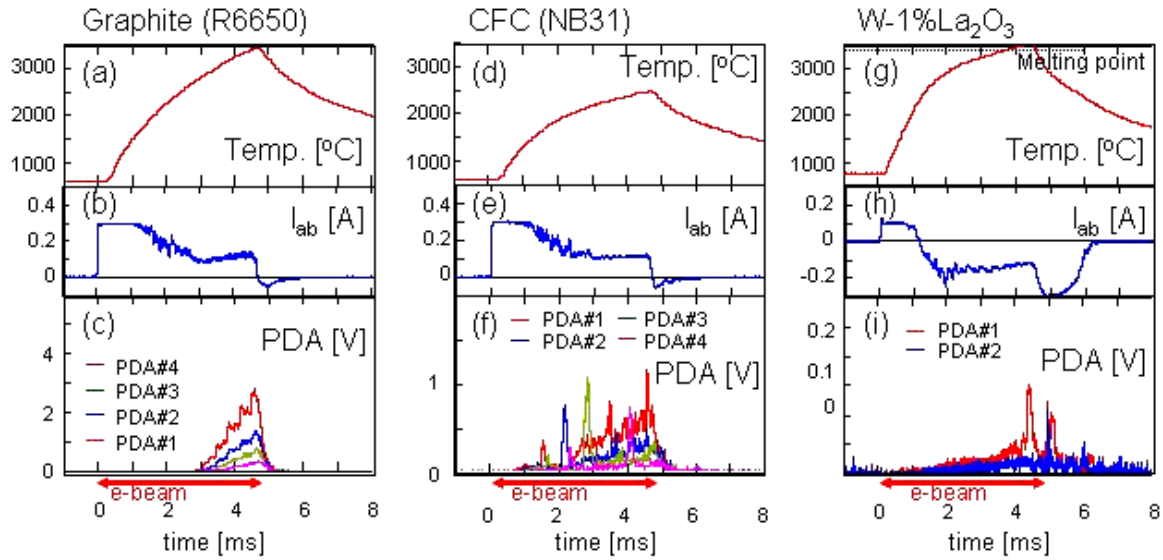
Fig.4, time evolution of surface temperatures (Temp.), absorbed currents (Iab), PDA signals during thermal shock tests on (a) - (c) graphite, 2 GW/m^2, 4.6 ms, (d) - (f) CFC , 2 GW/m^2, 4.6 ms, (g) - (i) W-1%La$_2$O$_3$, 1.1 GW/m^2, 4.6 ms.
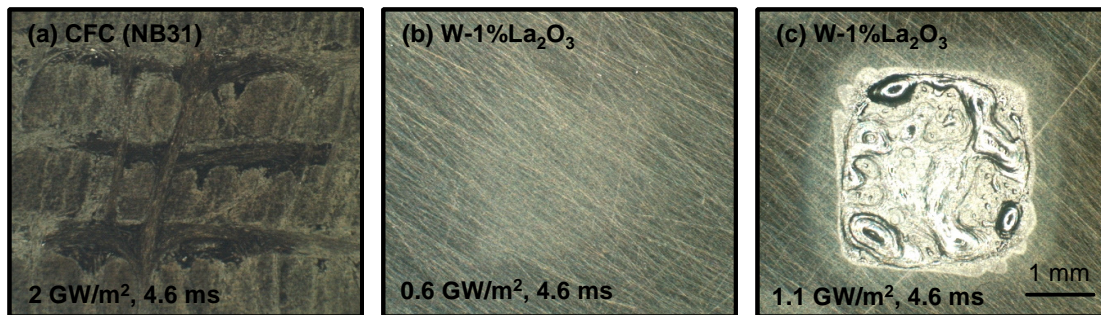

Fig.5, Microstructures of loaded surfaces. (a) CFC, 2 GW/m^2, 4.6 ms, (b) W-1%La$_2$O$_3$, 0.6 GW/m^2, (c) W-1%La^{2}O$_3$, 1.1 GW/m^2, 4.6 ms.

whereas, PAN fibers showed strong erosion as shown in Fig. 5(a). PDA signals in numbers of tests at the same condition showed that no particular initiation temperature (averaged surface temperature) where the particle release appeared as PDA signals. This also indicates that particle release started at local overheated points. The initiation temperature depends on the local structures and local thermal properties. Consequently, it is concluded that CFC would be suffered from macroscopic erosion because of local overheating associated with its inhomogeneous structure.

Figure 6 shows spectra in front of targets. Microscopic erosion, i.e. released atoms and molecules are observed by emission spectrometer. Figure 6(a) and (b) show spectra from the graphite and CFC samples, respectively. C$_2$ Swan bands and C$_3$ bands around 400 nm, were observed predominately [14,15]. Strong CII lines were observed in CFC, whereas, no CII lines were visible in graphite in this particular condition. This indicates that there were
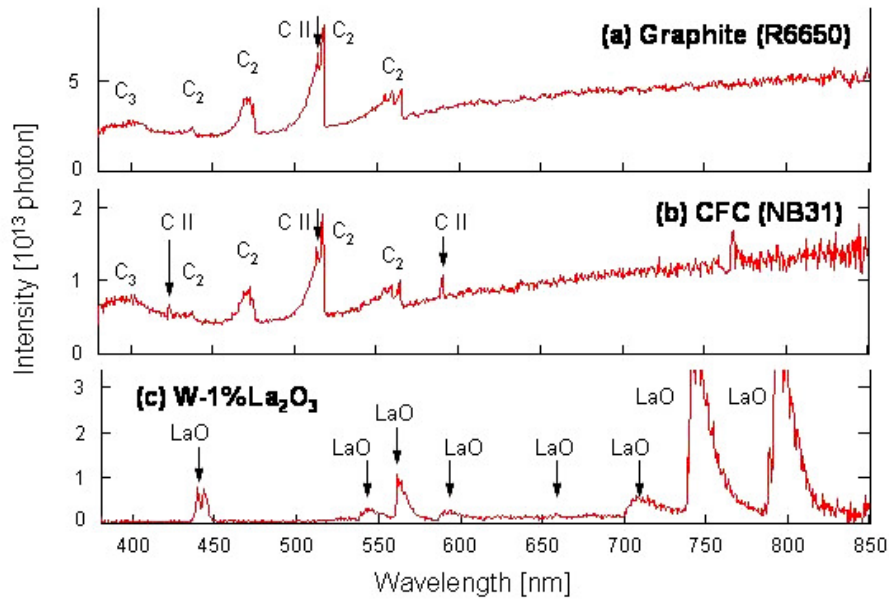
Fig.6, Spectra during thermal shock tests on (a) graphite, 2 GW/m^2, 4.6 ms, (b) CFC, 2 GW/m^2, 4.6ms, (c) W-1%La$_2$O$_3$, 0.6 GW/m^2, 4.6 ms.

differences in released species from targets by different surface morphology and/or excitation processes in front of target due to different surface temperatures [16].

3.2 Thermal shock tests on W-1%La$_2$O$_3$

Figure 3(c) shows time integral image during a thermal shock test on W-1%La$_2$O$_3$. Particle release was observed at 1.1 GW/m^2 for 4.6 ms as shown in the image. Most of the particles traces suddenly increased the intensity at a point traveling away from the surface, i.e. dark traces to bright traces. A possible reason is a sudden change of emissivity due to a phase change, possibly liquid to solid phase. As shown in Fig. 4(g), the surface temperature raised more than 3400°C which is the melting point of tungsten. Molten surface was observed at 1.1 GW/m^2 (Fig. 5(c)). PDA signals (Fig. 4(i)) showed also particle release during thermal shock tests. It was found that the particle release started at the very end of the shot when the measured surface temperature reached above 3000°C. These results indicate that most of the particles from W-1%La$_2$O$_3$ released after melting, namely, splashing of droplets. At a lower power density, 0.6 GW/m^2, no particle release was observed and the surface did not melt as depicted in Fig. 5(b). Accordingly, it is concluded that particle release from W-1%La$_2$O$_3$ was caused by splashing of the melted layer and particle release due to brittle destruction was not dominant in this particular condition. Figure 6(c) shows spectrum obtained in front of W-1%La$_2$O$_3$ target at a power density 0.6 GW/m^2 for 4.6 ms. Tungsten atom, WI lines (e.g. 400 nm) and WO bands were not observed even at the higher power density, 1.1 GW/m^2 which caused surface melting. However, LaO molecular bands [14] were clearly observed even in this low power density, 0.6 GW/m^2 where the surface temperature arrived at around

2500 ^{o}C and the surface did not show significant modification. It means that the La$_2$O$_3$ particles dispersed in the bulk tungsten dissociated below melting temperature of tungsten and released from the surface. In fact, La$_2$O$_3$ has melting temperature around 2300 ^{o}C. It was molten and evaporated during the thermal shock loads. As it is often observed in tungsten alloy, severe cracking was observed at the vicinity of the melting spots. Taniguchi et al reported that the weight loss of W-1%La$_2$O$_3$ was greater than that of pure tungsten at 1.25 GW/m^2 for 2 ms [17]. It indicates that adding La$_2$O$_3$ in tungsten does not mean improvement of tungsten performances and it causes introduction of additional impurity in vacuum chamber.

4. Summary

Dynamic erosion processes were observed by optical diagnostics in electron beam facility, JUDITH. Collective small particle release was observed in case of graphite, at 2 GW/m^2 for 4.6 ms, whereas, distinguished particle release was observed in case of CFC in the same condition. The distinguished particles from CFC were concluded to be segments of PAN fibers. W-1%La$_2$O$_3$ seemed to release mainly droplet due to melt layer splash. Contribution of brittle destruction in W-1%La$_2$O$_3$ under thermal shock tests was not clearly observed in this particular condition. Release of W atom and WO species was not observed even at 1.1 GW/m^2 which caused significant melting of the surfaces, however, release of LaO molecules were clearly detected even at low power density, 0.6 GW/m^2 where the surface did not show significant modification.

References

[1] FEDERICI, G., SKINNER, C. H., et al. Nucl. Fusion **41** (2001) 1967.
[2] LINKE, J., BOLT, H., DUWE, R., KÜHNLEIN, W., LODATO, A., RÖDIG, M., SCHÖPFLIN, K., WIECHERS, B., J. Nucl. Mater. **283-287** (2000) 1152-1156.
[3] LINKE, J., RUBEL, M., MALMBERG, J. A., DARKE, J. R., DUWE, R., PENKALLA, H.-J., RÖDIG, M., WESSEL, E., Physica Scripta **T91** (2001) 36-42.
[4] LINKE, J., AKIBA, M., DUWE, R., LODATO, A., PENKALLA, H.-J., RÖDIG, M., SCHÖPFLIN, K., J. Nucl. Mater. **290-293** (2001) 1102-1106.
[5] LINKE, J., AMOUROUX, S., BERTHE, E., KOZA, Y., KÜHNLEIN, W., RÖDIG, M.,

Fusion Eng. Des. **66-68** (2003) 395-399.

[6] KOZA, Y., BERTHE, E., LEHMANN, E., LINKE, J., RÖDIG, M., WESSEL, E., SINGHWISER, L., J. Nucl. Mater. **329-333** (2004) 706-710.

[7] KOZA, Y., AMOUROUX, S., BAZYLEV, B. N., BERTHE, E., KÜHNLEIN, W., LINKE, J., PENKALLA, H.-J., SINGHEISER, L., Physica Scripta **T111** (2004) 167-172.

[8] HIRAI, T., LINKE, J., KÜHNLEIN, W., SERGIENKO, G., BREZINSEK, S., J. Nucl. Mater. **321** (2003) 110–114.

[9] HIRAI, T., BREZINSEK, S., KÜHNLEIN, W., LINKE J., SERGIENKO, G., Physica Scripta **T111** (2004) 163-166.

[10] DUWE, R., KÜHNLEIN, W., MÜNSTERMANN, H., Proc. 18th Symposium on Fusion Thechnology (SOFT), Karlsruhe Germany, (1994) p.355.

[11] TANIGUCHI, M., SATO, K., EZATO, K., YOKOYAMA, K., AKIBA, M., J. Nuclear Material, **307-311**, (2002) 719-722.

[12] RÖDIG, M., ISHISTUKA, E., GARACASH, A., KAWAMURA, H., LINKE, J., LITUNOVSKI, N., MEROLA, M., J. Nucl. Mater. **307-311** (2002) 53-59.

[13] ARKHIPOV, N., BAKHTIN, V., BARSUK, V., KURKIN, S., MIRONOVA, E., PIAZZA, G., SAFRONOV, V., SCAFFIDI-ARGENTINA, F., TOPORKOV, D., VASENIN, S., WÜRZ, H., ZHITLUKHIN, A., J. Nucl. Mater. **307-311** (2002) 1364-1368.

[14] PEARSE, R. E. B., GAYDON, A. G., "The idensification of molecular spectra" John Wiley & Sons, Inc. New York, 1976.

[15] AREPALLI, S., SCOTT, C. D., Chem. Phys. Lett. **302** (1999) 139-145.

[16] JANEV, R. K., DRAWIN, H. W., Atomic and Plasma–Material Interaction Process in Controlled Thermonuclear Fusion, Elsevier, Amsterdam, 1993, p. 213.

[17] TANIGUCHI, M., SATO, K., EZATO, K., MASAKI, K., NAKAMURA, K., MIYA, N., ARAKI, M., AKIBA, M., Fusion Technology **39** (2001) 890.